CHAPTER 3

MORPHOLOGY AND MECHANICAL PROPERTIES OF NBR/EVA BLENDS

The results of this chapter have been published in
(i) *Eur. Polym. J.*, **31**, 957 (1995) and
(ii) *Mater. Lett.*, **24**, 333 (1995)

Tailoring of polymer properties through blending different polymers has long been recognised as a viable method to meet specific applications.[1,2] The resultant properties of polymer blends depend on the proportion and properties of the individual polymeric components as well as the mode of dispersion and interaction between the phases. The major factors affecting blend morphology are volume fraction and viscosity. Danesi and Porter[3] have shown that for the same processing conditions the blend morphology is determined by the composition ratio and melt viscosity difference of the components. Continuity of a phase is favoured by high volume fraction and low viscosity relative to that of the other component. It has been reported that the properties of polymer blends are strongly influenced by the morphology of the system.[4-6] The influence of blend morphology on mechanical behaviour of rubber-toughened diglycidyl ether of bisphenol-A epoxy was reported by Bagheri and Pearson.[5] Cimmino *et al.*[6] have related the mechanical properties of binary polyamide 6/rubber blends with the blend morphology.

The influence of blend composition on the morphology and mechanical properties of NBR/EVA blends is discussed in this chapter. The morphology of the blend is analysed by both optical and scanning electron microscopes. The correlation between properties and morphology of the system is also carried out.

3.1 Results and discussion

3.1.1 Morphology of the blends

The optical micrographs of the blends are shown in Figure 3.1. In N_{10}, N_{20} and N_{30} (Figures 3.1a–c), NBR is dispersed in EVA matrix. Correspondingly in N_{70}, N_{80} and N_{90} (Figures 3.1g–i) EVA is the dispersed phase in NBR matrix but with a larger domain size. This is due to the clustering of EVA domains as reported in the case of NR/EVA blends.[7] Occurrence of coalescence at higher concentrations of one of the components has been reported by many authors.[8-12] In the case of polyethylene/polystyrene blends, the increase in domain dimension of PE at its higher concentration is caused by coalescence.[9] Thomas *et al.*[10,11] have reported similar phenomenon in the case of hytrel/PVC and EVA/PP blends.

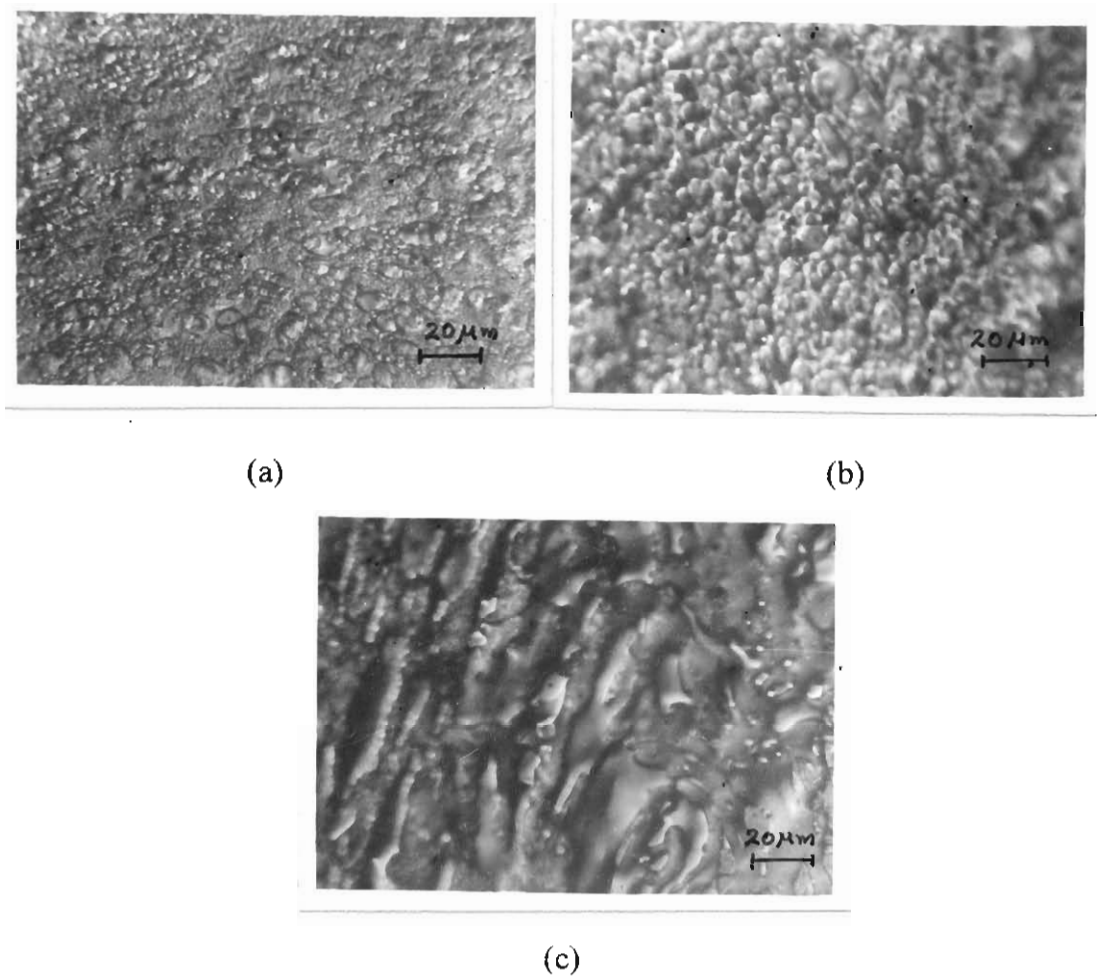

(a) (b)

(c)

Figure 3.1. Optical micrographs showing the blend morphology of different blend compositions; (a) N_{10}, (b) N_{20} and (c) N_{30}

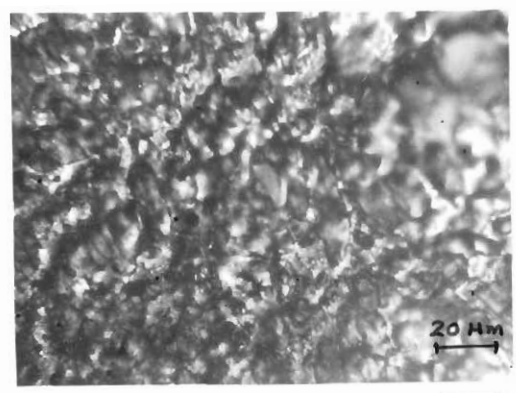

(d)

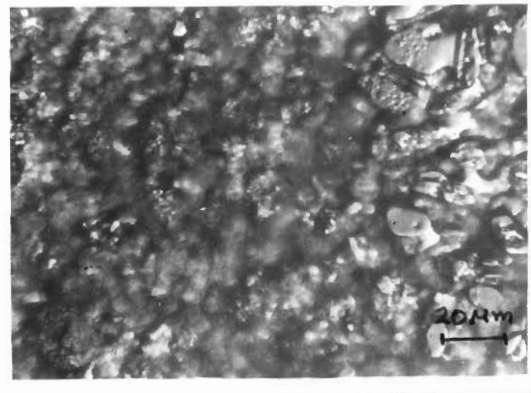

(e)

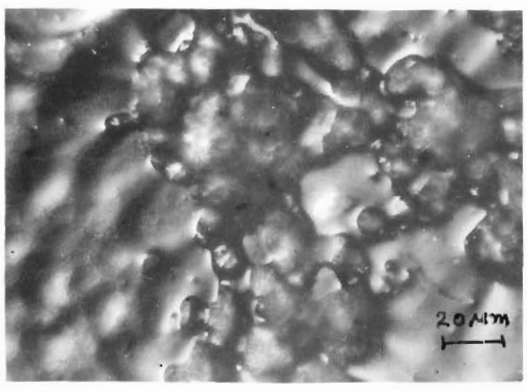

(f)

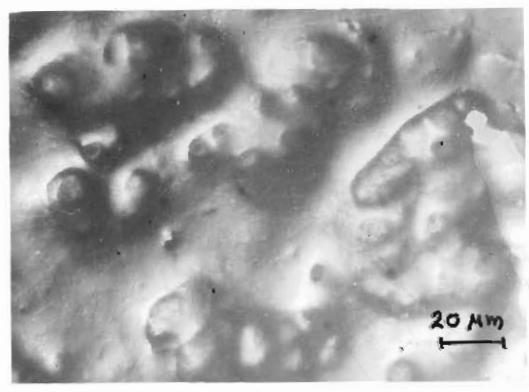

(g)

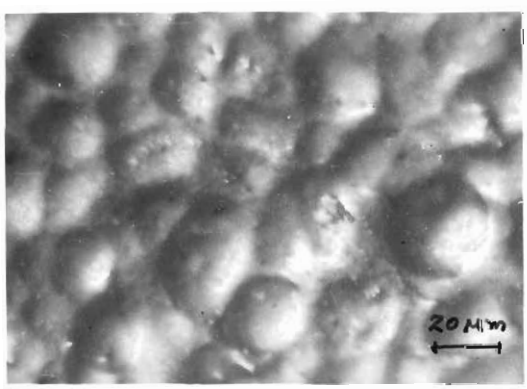

(h)

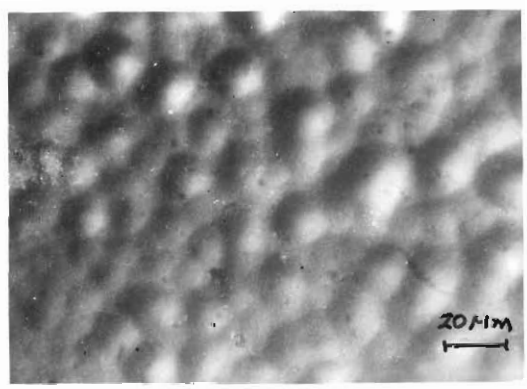

(i)

Figure 3.1. Optical micrographs showing the blend morphology of different blend compositions: (d) N_{40}, (e) N_{50}, (f) N_{60}, (g) N_{70}, (h) N_{80} and (i) N_{90}

In N_{40}, N_{50} and N_{60} (Figures 3.1d–f) both the phases exist as continuous phases (co-continuous morphology).

The scanning electron micrographs of a few blend compositions are given in Figure 3.2. The elongated nature of the dispersed particles in N_{30} (Figure 3.2a) could be understood from the scanning electron micrograph. In N_{30} and N_{70} (Figures 3.2a and 3.2c), the minor component is dispersed within a continuum of the major component. N_{50} (Figure 3.2b) exhibits a co-continuous morphology in which both the components are continuous.

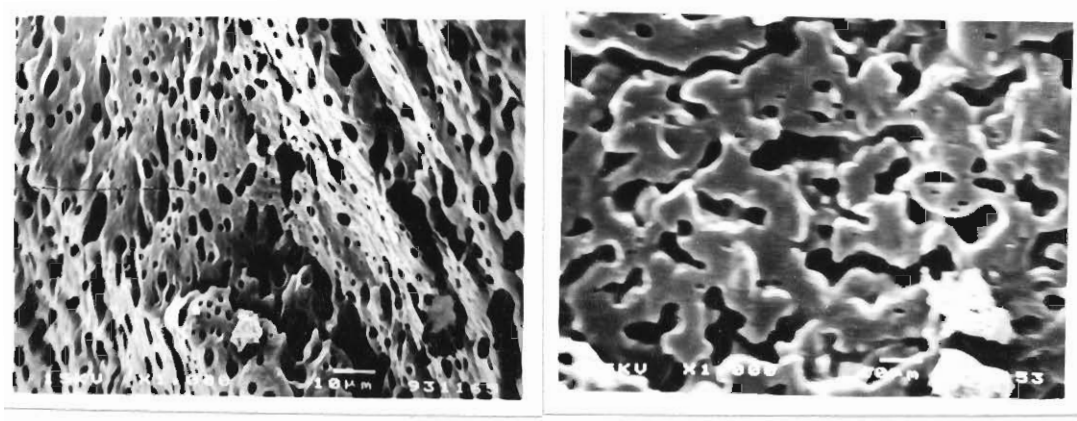

(a) (b)

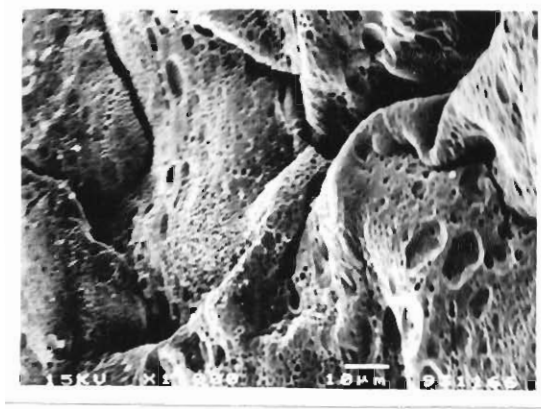

(c)

Figure 3.2. Scanning electron micrographs showing the microstructure morphology of (a) N_{30}, (b) N_{50} and (c) N_{70}

The average particle size as a function of blend composition is shown in Figure 3.3. In the blends with high EVA content, NBR is the dispersed phase and

the average particle size of the dispersed domains increases with increase in NBR content. In NBR rich blends, the average particle size of the dispersed EVA domains increases with increase in EVA content. The increase in domain size of NBR or EVA with increasing proportion of that component is associated with the coalescence or recombination of the domains.[7-12] Between 40 and 60 weight per cent of NBR a co-continuous morphology is observed for the blend.

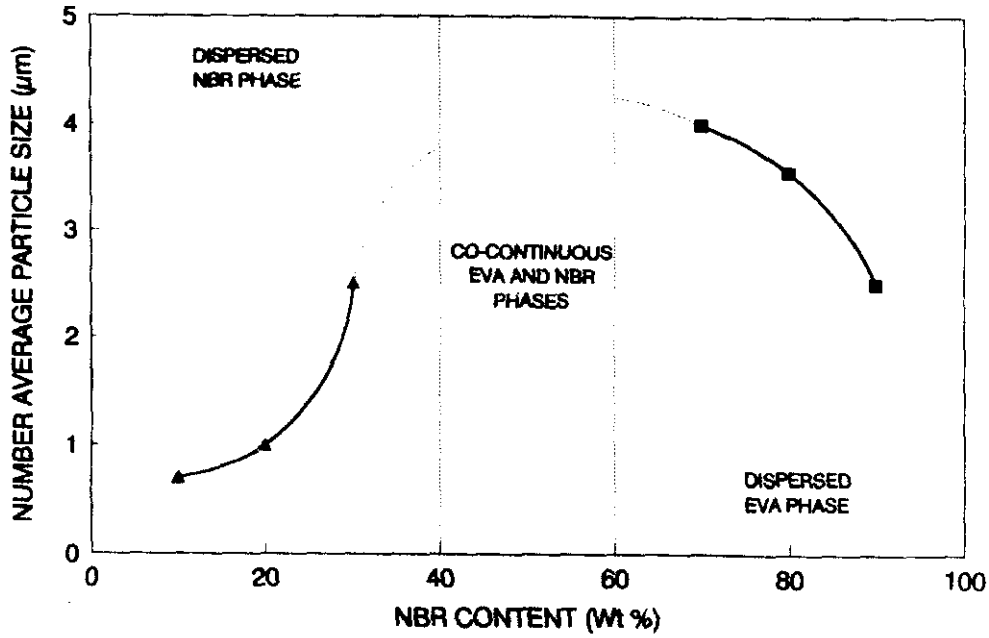

Figure 3.3. Effect of blend composition on the dispersed particle size

From the optical micrographs of the blends, the particle size distribution curves are generated by measuring the domain size of the dispersed phase (200 particles in each case) and is shown in Figure 3.4. It is observed that the blend N_{90} (90/10:NBR/EVA) exhibits a broader distribution than N_{10} (10/90:NBR/EVA). This is attributed to the clustering of EVA particles in the former blend. In the case of N_{30} and N_{70} nearly same distribution is observed.

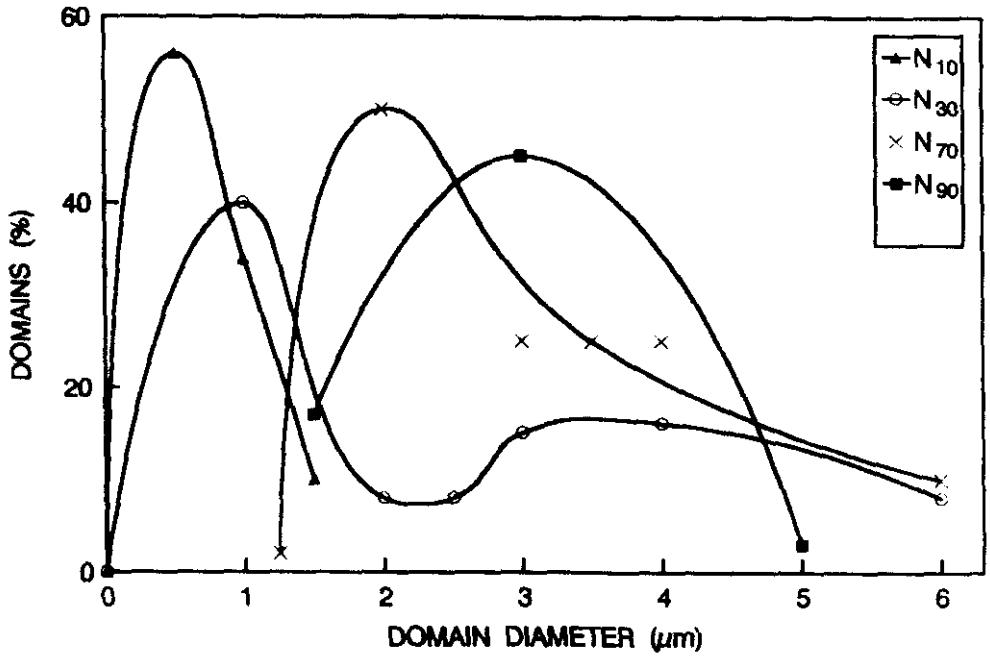

Figure 3.4. Particle size distribution curves of NBR/EVA blends

3.1.2 Mechanical properties

The stress-strain curves of NBR/EVA blends are shown in Figure 3.5. The differences in deformation characteristics of the individual polymers and blends under an applied load are evident from the stress-strain curves. Pure EVA and EVA rich blends show higher initial modulus with yield point. At higher strains these blends show a gradual increase in stress which can be attributed to the orientation of the polyethylene crystalline hard segments of EVA, the continuous phase, in the direction of applied load. The stress-strain curves of pure EVA and EVA rich blends show distinct elastic and inelastic regions. In the inelastic region, the samples undergo yielding and strain induced crystallisation. The stress-strain curve of NBR (N_{100}) exhibit typical uncrosslinked elastomeric behaviour. In the blends, N_{70} and N_{90}, where NBR is the continuous phase, a similar stress-strain behaviour as that of NBR is observed. The N_{50} with a co-continuous morphology

shows a stress-strain behaviour which is intermediate to those of the other blend compositions.

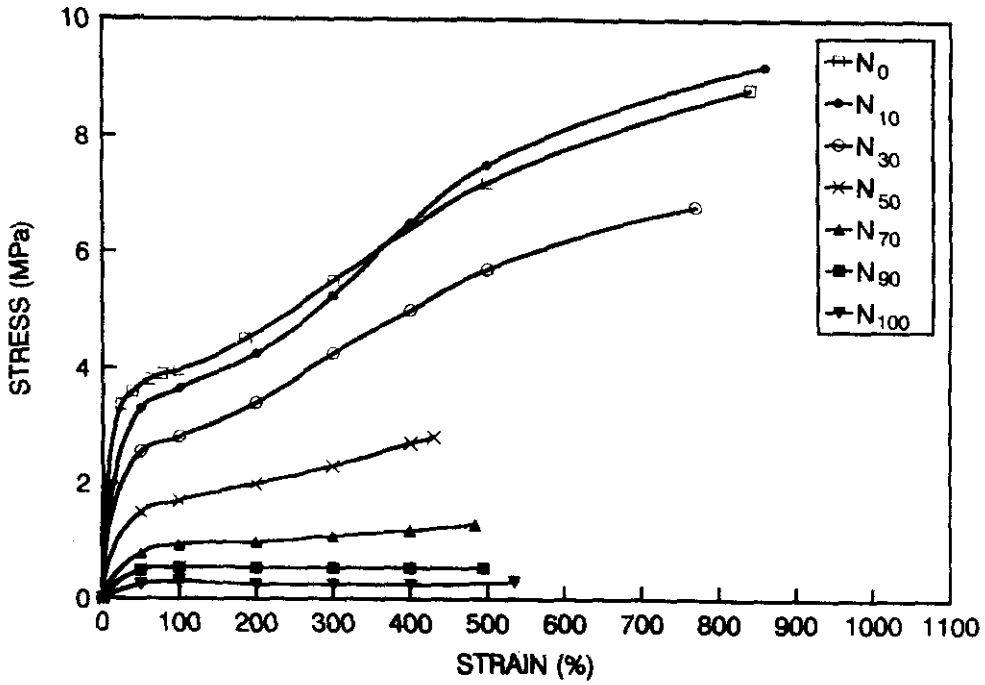

Figure 3.5. Stress-strain behaviour of NBR/EVA blends

In Figure 3.6 Young's modulus and stress at 100% elongation are plotted as a function of the weight percentage of EVA. The Young's moduli of the blends increase with EVA content. The increase in stress at 100% elongation is less marked at the extreme ends of the curve compared to that at the middle portion. Elongation at break, tensile strength and hardness increase with the weight percentage of EVA (Figures 3.7 and 3.8). In all these curves the properties increase more sharply when the EVA content is more than 40%. This is due to the fact that when the weight percentage of EVA is more than 40%, it tends to become the continuous phase.

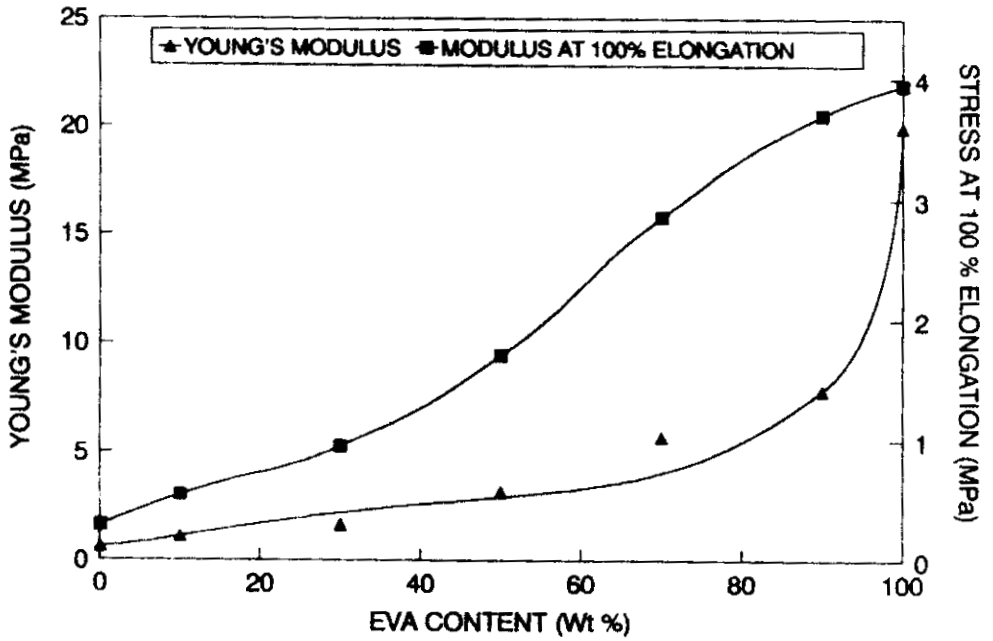

Figure 3.6. Variation of Young's modulus and stress at 100% elongation as a function of weight per cent of EVA in the blend

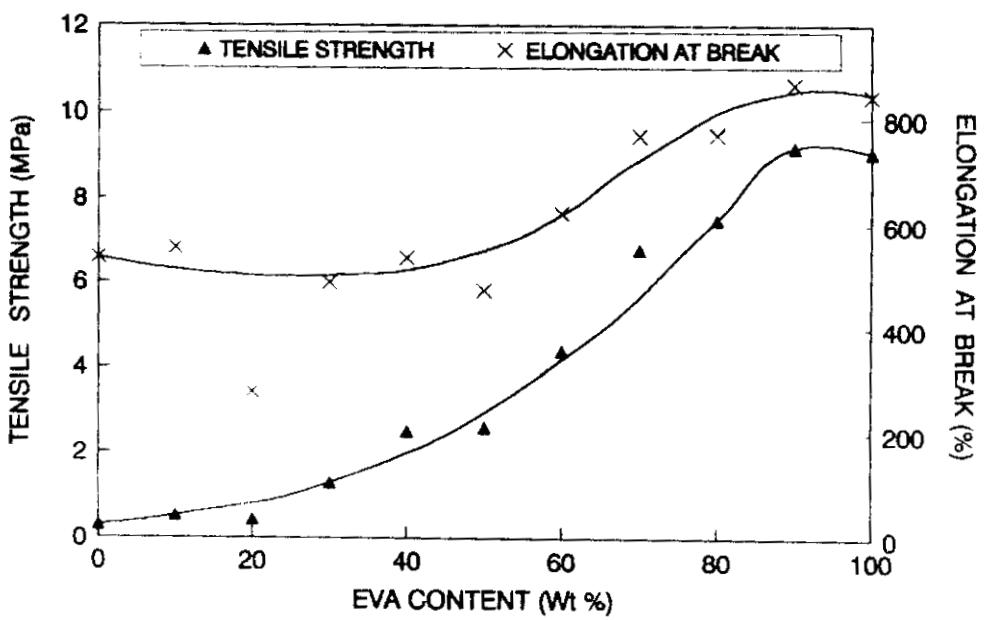

Figure 3.7. Variation of tensile strength and elongation at break as a function of weight per cent of EVA in the blend

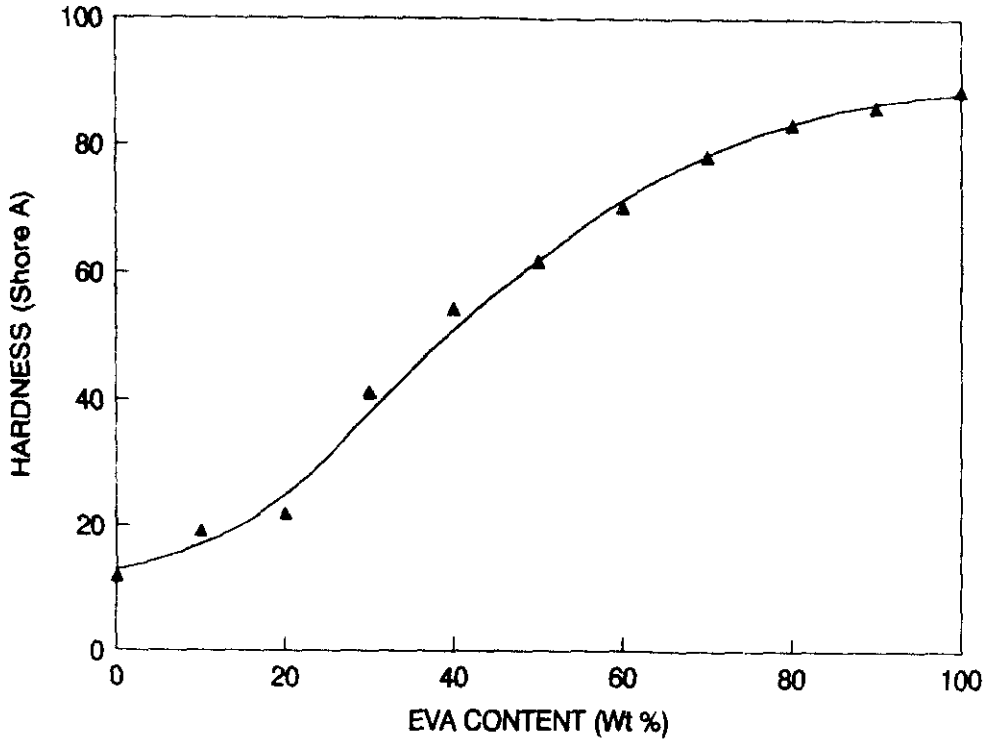

Figure 3.8. Effect of EVA content on the hardness of NBR/EVA blends

Figure 3.9 shows the variation of tear strength of the blends as a function of weight per cent of NBR. It is seen that the tear strength values decrease with the weight per cent of NBR, i.e., the strength of NBR/EVA blends depends on the strength of EVA, which in turn depends on the crystallinity of EVA. It is reported that the crystallinity of a material is reduced in the presence of rubber particles.[11,13] Thomas *et al.* have studied the crystallinity of natural rubber (NR)/ethylene-vinyl acetate (EVA) copolymer blends using X-ray diffraction (XRD).[14] They observed that addition of NR to EVA results in increase in interplanar distance between crystallites. This is attributed to the migration of NR phase into the interchain spaces of EVA. Thus the observed decrease in tear strength in NBR rich blends may also be attributed to the decrease in crystallinity of the EVA phase. The NBR rich region shows a negative deviation from the additivity line i.e., there is a clear

change in slope from 40 weight per cent of EVA onwards. This is due to the phase inversion in the morphology of the system as observed from the optical and scanning electron micrographs (Figures 3.1 and 3.2). Up to 30 weight per cent of EVA, NBR is the continuous phase and EVA, the dispersed phase. From 40 to 60 weight per cent of EVA, both phases are continuous and thereafter EVA tends to become the continuous phase and NBR, the dispersed phase.

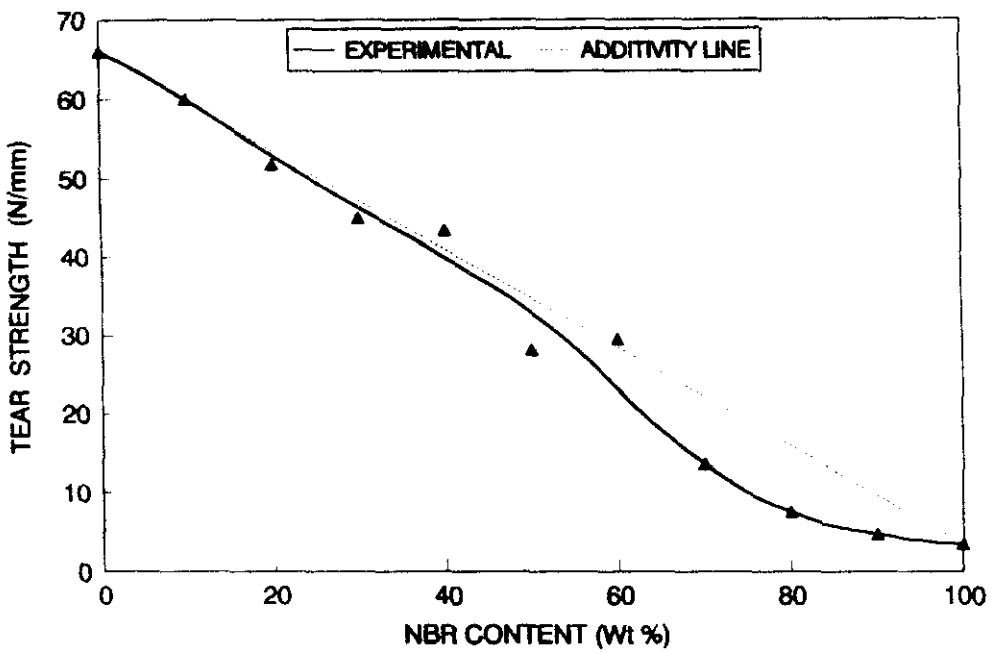

Figure 3.9. Variation of tear strength as a function of weight per cent of NBR in the blend

The tear curves (load vs. displacement) of the blends are given in Figure 3.10. EVA exhibits the highest tear force and the least extension. It is observed from the figure that the tear strength increases with EVA content in the blend. This indicates that EVA enhances the resistance to tearing of all samples. It is seen that the displacement increases with decrease in EVA content (except in the case of 50/50 blend). Thus, NBR with the lowest tear strength shows the highest

displacement and lowest tearing force. The high displacement is due to the yielding of the rubber phase.

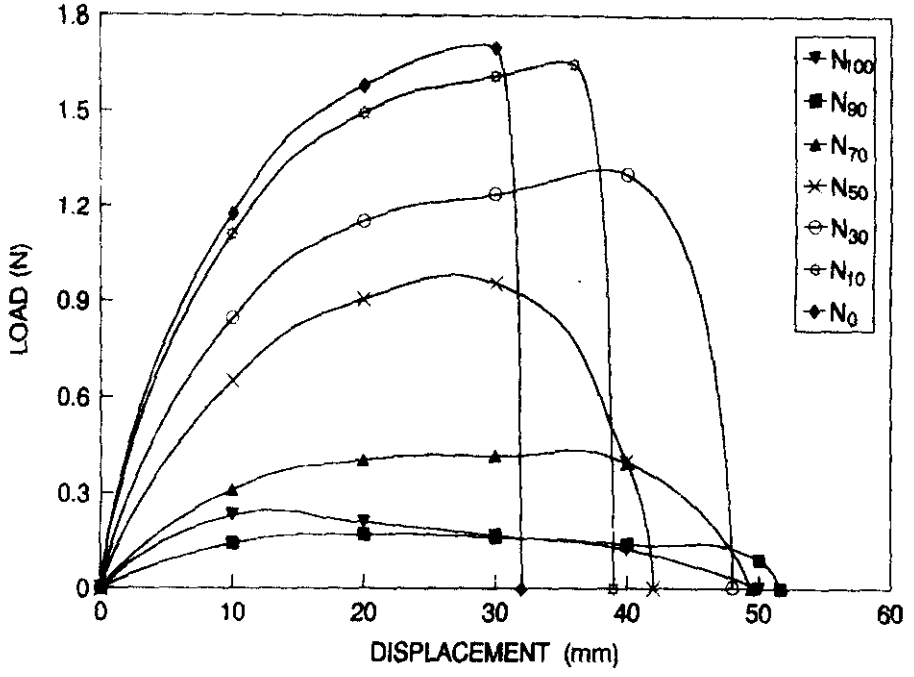

Figure 3.10. Load-displacement curves of NBR/EVA blends

To understand the tear failure process, tear fractographs shown in Figure 3.11 of the fracture surfaces are obtained using a scanning electron microscope. EVA which exhibits the highest tear strength shows tear "fronts" growing sinusoidally along wavy crests and troughs (Figure 3.11a). The sinusoidal folds and striations are very close. These are characteristic of materials having high tear strength Similar observations were made in the case of 1,2-polybutadiene and thermoplastic copolyester elastomer,[15,16] both of which exhibit very high tear strength.

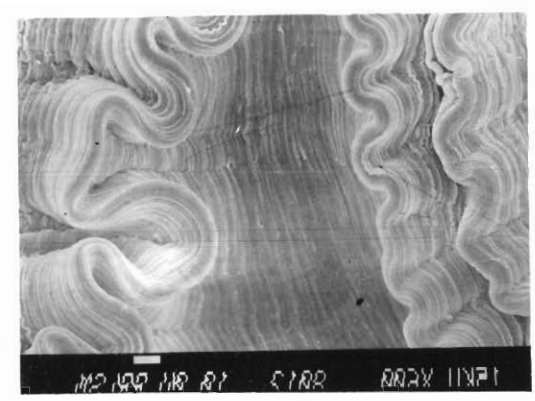

(a)

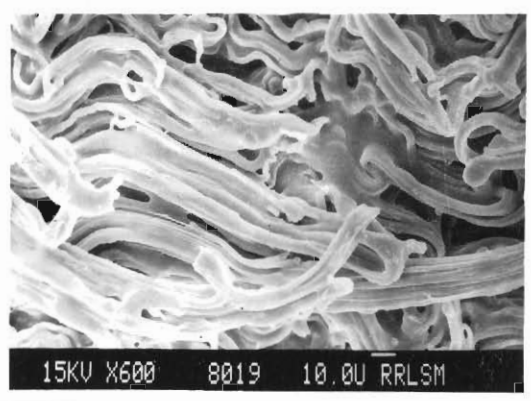

(b)

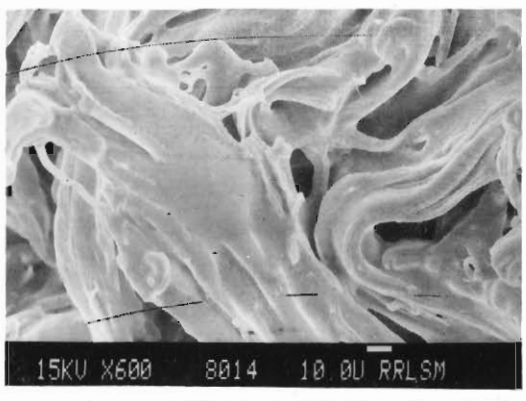

(c)

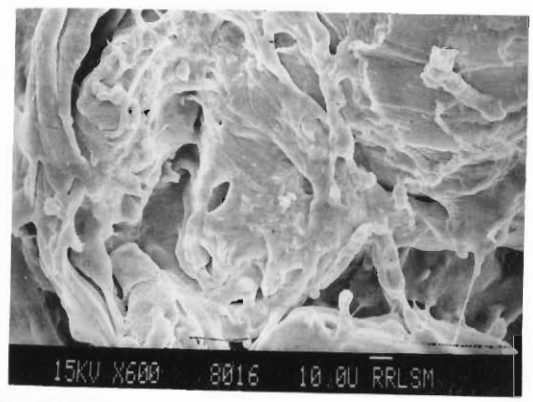

(d)

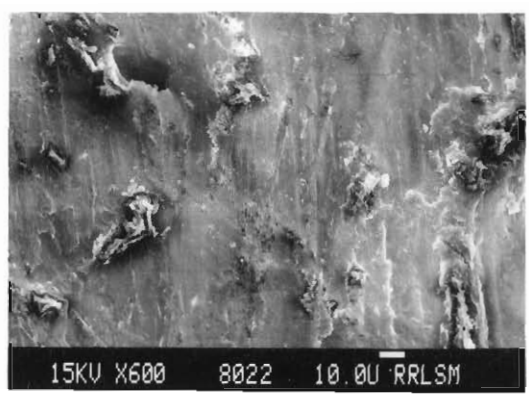

(e)

Figure 3.11. Scanning electron micrographs showing the tear fronts of (a) N_0, (b) N_{30}, (c) N_{50}, (d) N_{70}, and (e) N_{100}

The tear strength of polymers was related to the morphological features of the fracture surface by Gent and Pulford.[17] They measured the step spacing on the fracture surface and found that strong materials show more closely spaced steps. Smooth torn areas were seen in the case of weak materials. It can be concluded from the earlier reports that a significant sinusoidal wavy pattern at the fracture surface is a characteristic feature of materials having high tear resistance.[17-19] The plastic deformation of EVA (N_0) gives rise to such a pattern due to the extensive stretching of the matrix along the direction of applied load. The average distance between the two adjacent sinusoidal folds is approximately equal to 13 μm. The tear strength of the blends decreases with the addition of nitrile rubber. In N_{30} the sinusoidal wavy pattern disappeared (Figure 3.11b). It exhibits some fibrillar structure indicating a certain extent of plastic deformation. In N_{50} the fibrillar structure diminishes and shows a relatively rough surface (Figure 3.11c). The torn surface becomes somewhat smooth in the case of N_{70} (Figure 3.11d). The tear front of N_{100} exhibits very smooth torn areas which is the characteristic feature of weak materials (Figure 3.11e).

3.1.3 *Model fitting*

Applicability of various composite models such as parallel, series, Halpin-Tsai, Coran's, Takayanagi, Kerner and Kunori is examined to predict the mechanical behaviour of the blends.

The parallel model (highest-upper-bound model) is given by the equation,[1,20]

$$M = M_1\phi_1 + M_2\phi_2 \qquad (3.1)$$

where M is the mechanical property of the blend and M_1 and M_2 are the mechanical properties of the components 1 and 2 respectively and ϕ_1 and ϕ_2 are the volume fractions of the components 1 and 2 respectively. In this model the components are considered to be arranged parallel to one another so that the applied load stretches each of the component by the same amount.

In the lowest-lower-bound series model, the components are arranged in series with the applied stress. The equation is[1,20]

$$1/M = \phi_1/M_1 + \phi_2/M_2 \quad (3.2)$$

According to Halpin-Tsai equation[21]

$$M_1/M = (1+ A_iB_i\phi_2)/(1- B_i\phi_2) \quad (3.3)$$

$$B_i = (M_1/M_2 - 1)/(M_1/M_2 + A_i) \quad (3.4)$$

In this equation the subscripts 1 and 2 refer to the continuous and dispersed phase, respectively. The constant A_i is defined by the morphology of the system. For elastomer domains dispersed in a hard continuous matrix, $A_i = 0.66$.

In Coran's model, the mechanical properties are generally in between the parallel model upper bound (M_U) and the series model lower bound (M_L).

According to Coran's equation,[22]

$$M = f(M_U - M_L) + M_L \quad (3.5)$$

where f can vary between zero and unity. 'f' is a function of phase morphology and is given by

$$f = V_H^n(nV_S + 1) \quad (3.6)$$

where n contains the aspects of phase morphology. V_H and V_S are the volume fraction of the hard phase and soft phase respectively.

According to Takayanagi model[23,24]

$$M = (1 - \lambda) M_1 + \lambda[(1-\phi)/M_1 + (\phi/M_2)]^{-1} \quad (3.7)$$

M_1 is the property of the matrix phase, M_2 is the property of the dispersed phase and $\phi\lambda$ is the volume fraction of the dispersed phase and is related to the degree of series-parallel coupling. The degree of parallel coupling of the model can be expressed by

$$\% \text{ parallel} = [\phi(1-\lambda)/(1-\phi\lambda)] \times 100 \quad (3.8)$$

According to Kerner model[25,26]

$$E_b = E_m \left[\frac{\phi_d E_d / \left[(7-5\nu_m)E_m + (8-10\nu_m)E_d\right] + \phi_m / 15(1-\nu_m)}{\phi_d E_m / \left[(7-5\nu_m)E_m + (8-10\nu_m)E_d\right] + \phi_m / 15(1-\nu_m)} \right] \quad (3.9)$$

where E_b is the blend property, ν_m is the Poisson's ratio and ϕ is the volume fraction. The subscripts m, d and b stand for the matrix, dispersed phase and blend, respectively.

According to Kunori *et al.*[27] tensile failure of a blend is the result of adhesion failure between the blend components. When there is no adhesive force between the blend components, the tensile strength of the blends, σ_b, may be written as:

$$\sigma_b = \sigma_m (1-A_d) \quad (3.10)$$

where σ_b and σ_m are the tensile strength of the blends and the matrix respectively and A_d represents the area occupied by the dispersed phase in transverse cross-section. Kunori *et al.*[27] assumed that when a strong adhesive force exists between the blend components the dispersed phase will contribute to the strength of the blend and therefore parallel model may be modified as follows:

$$\sigma_b = \sigma_m (1-A_d) + \sigma_d A_d \quad (3.11)$$

If the force propagates mainly through the interface the above equation may be written as:

$$\sigma_b = \sigma_m (1-\phi_d^{2/3}) + \sigma_d \phi_d^{2/3} \quad (3.12)$$

and if the force propagates through the matrix then the equation becomes:

$$\sigma_b = \sigma_m (1-\phi_d) + \sigma_d \phi_d \quad (3.13)$$

The applicability of these models to predict Young's modulus of the blends is presented in Figure 3.12. It is observed that the experimental values lie close to the series model. This may be attributed to the simple morphological arrangement of components in the blend.

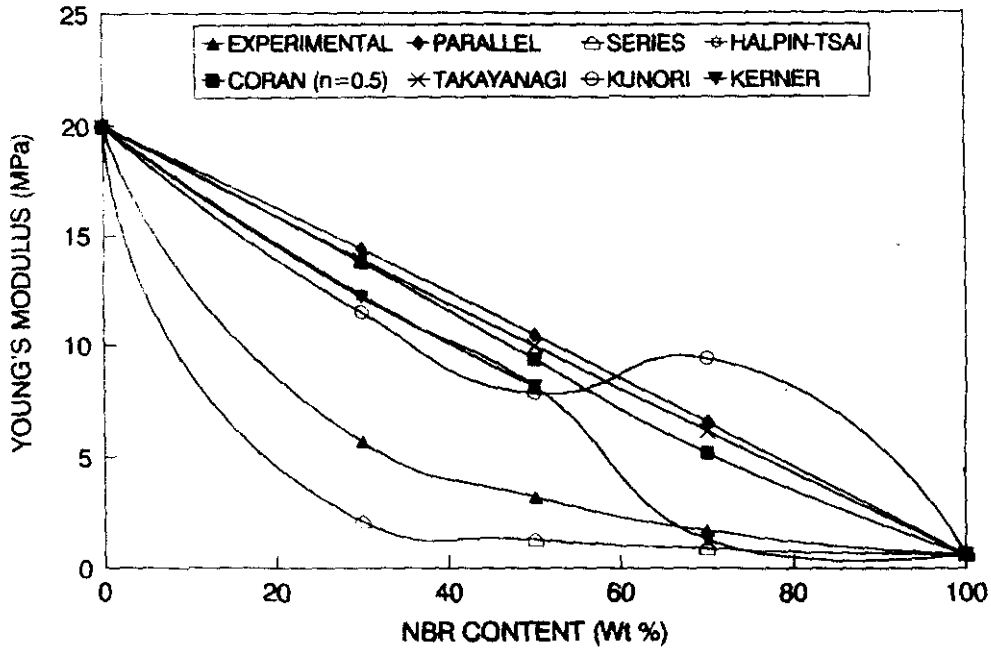

Figure 3.12. Applicability of various models for predicting modulus of NBR/EVA blends

3.1.4 Reprocessability of the blends

To study the reprocessability, the blends are subjected to repeated moulding up to 3 times at 150°C and the properties such as tensile strength, elongation at break and modulus are measured. In compression moulding, the shear is of low order (1-10 sec^{-1}) and hence the effect of shear on the properties of NBR/EVA blends is negligible. The variation in properties against the number of cycles is presented in Figures 3.13-3.15.

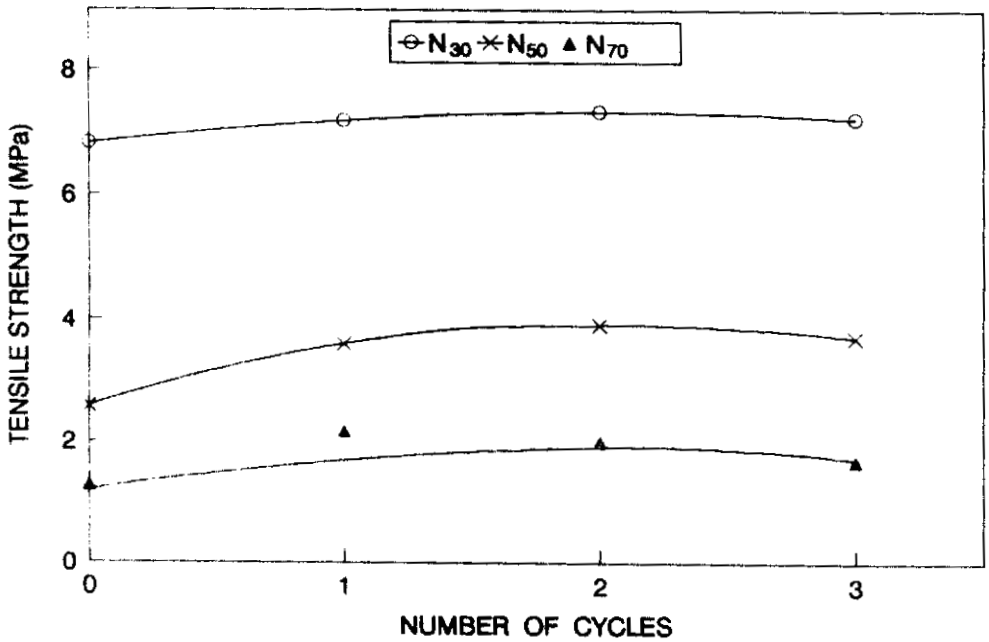

Figure 3.13. Effect of recycling on tensile strength of NBR/EVA blends

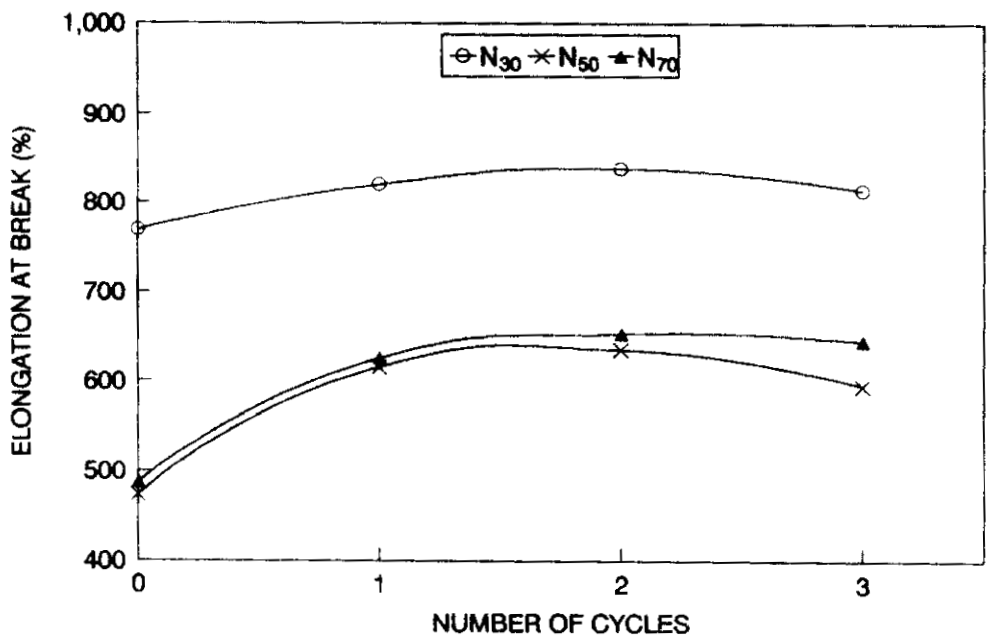

Figure 3.14. Effect of recycling on elongation at break of NBR/EVA blends

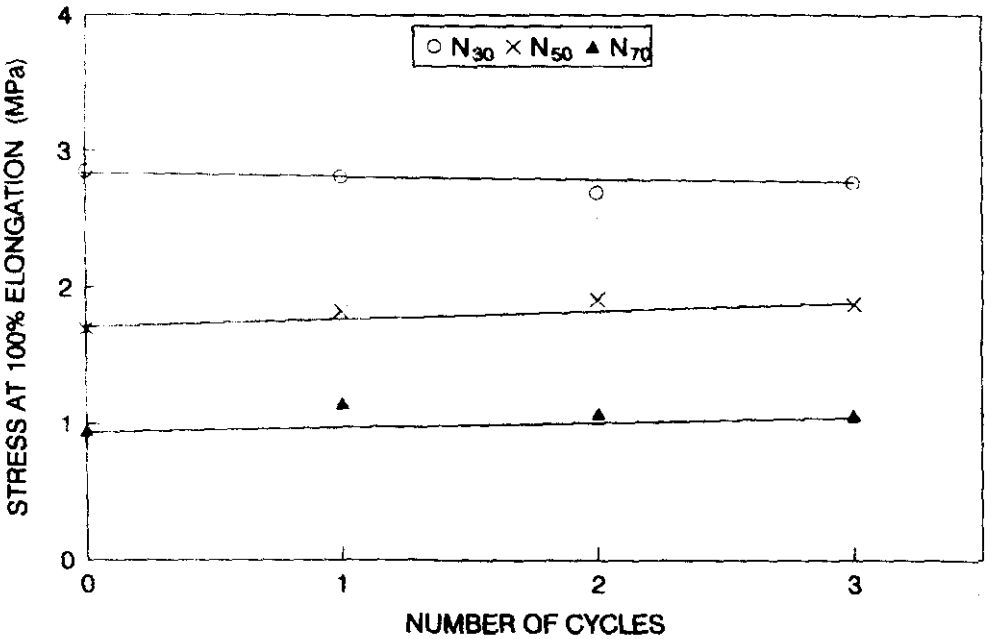

Figure 3.15. Effect of recycling on stress at 100% elongation of NBR/EVA blends

The tensile strength and elongation at break increase marginally for the second cycle and thereafter remain constant. This is due to the homogeneity in mixing achieved during reprocessing. The stress values remain constant throughout the recycling process. These results suggest that the blends can be recycled and reprocessed several times without adversely affecting the properties.

3.2 References

1 D. R. Paul and S. Newman, *Polymer Blends—Vols. 1 and 2*, Academic Press, New York, 1978.

2 O. Olabisi, C. M. Robeson and M. T. Shaw, *Polymer-Polymer Miscibility*, Academic Press, New York, 1979.

3 S. Danesi and R. S. Porter, *Polymer*, **19**, 448 (1978).

4 M. Baer, *J. Appl. Polym. Sci.*, **16**, 1109 (1972).

5 R. Bagheri and R. A. Pearson, *J. Mater. Sci.*, **31**, 3945 (1996).

6 S. Cimmino, L. D'orazio, R. Greco, G. Maglio, M. Malinconico, C. Mancarella, E. Martuscelli, R. Palumbo and G. Ragosta, *Polym. Eng. Sci.*, **24**, 48 (1984).

7. A. T. Koshy, *Ph.D. Thesis*, Submitted to Mahatma Gandhi University, Kottayam, India, 1991.

8. K. C. Dao, *Polymer*, **25**, 1527 (1984).

9. D. Heikens and W. Barentsen, *Polymer*, **18**, 69 (1977).

10. S. Thomas, B. R. Gupta and S. K. De, *J. Vinyl Technol.*, **9**, 71 (1987).

11. S. Thomas, S. K. De and B. R. Gupta, *Kauts. Gummi Kunst.*, **40**, 665 (1987).

12. Z. K. Walczak, *J. Appl. Polym. Sci.*, **17**, 169 (1973).

13. E. Martuscelli, C. Silverstre and G. Abate, *Polymer*, **23**, 229 (1982).

14. A. T. Koshy, B. Kuriakose, S. Thomas and S. Varghese, *Polymer*, **34**, 3428 (1993)

15. S. S. Bhagawan, D. K. Tripathy and S. K. De, *J. Mater. Sci.*, **6**, 157 (1987).

16. S. Thomas, B. Kuriakose, B. R. Gupta and S. K. De, *J. Mater. Sci.*, **21**, 711 (1986).

17. A. N. Gent and C. T. R. Pulford, *J. Mater. Sci.*, **19**, 3612 (1984).

18. B. Kuriakose and S. K. De, *J. Mater. Sci.*, **20**, 1864 (1985).

19. K. T. Varughese, G. B. Nando, S. K. De and S. K. Sanyal, *J. Mater. Sci.*, **24**, 3491 (1989).

20. S. Thomas and A. George, *Eur. Polym. J.*, **28**, 1451 (1992).

21. L. E. Nielson, *Rheol Acta*, **13**, 86 (1974).

22. A. Y. Coran, *Hand Book of Elastomers*, New Development and Technology, (Eds., A. K. Bhowmick and H. L. Stephens), Marcel Dekker, New York, 1988, p. 249

23. R. A. Dickie, *J. Appl. Polym. Sci.*, **17**, 45 (1973).

24. R. M. Holsto-Miettiner, J. Y. Seppala, O. T. Ikkala and I. T. Reima., *Polym. Eng. Sci.*, **34**, 395 (1994).

25. E. H. Kerner, *Proc. Phy. Soc.*, **69B**, 808 (1956).

26. G. G. Bandyopadhyay, S. S. Bhagawan, K. N. Ninan and S. Thomas, *Rubber Chem. Technol.*, **70(4)**, 650 (1997).

27. T. Kunori, P. H. Geil, *J. Macromol*, **218**, 36 (1960).